論文 / 著書情報
Article / Book Information

Title	Melting Experiments on Liquidus Phase Relations in the Fe‐S‐O Ternary System Under Core Pressures
Authors	Shunpei Yokoo, Kei Hirose, Ryosuke Sinmyo, Shoh Tagawa
Citation	Geophysical Research Letters, Vol. 46, Issue 10, pp. 5137-5145
Pub. date	2019, 4
DOI	https://doi.org/10.1029/2019GL082277
Copyright	(c) 2019 American Geophysical Union (AGU)

Geophysical Research Letters

RESEARCH LETTER
10.1029/2019GL082277

Melting Experiments on Liquidus Phase Relations in the Fe-S-O Ternary System Under Core Pressures

Shunpei Yokoo[1], **Kei Hirose**[1,2], **Ryosuke Sinmyo**[1], **and Shoh Tagawa**[1]

[1]Department of Earth and Planetary Science, The University of Tokyo, Tokyo, Japan, [2]Earth-Life Science Institute, Tokyo Institute of Technology, Tokyo, Japan

Key Points:
- Liquidus phase relations in the Fe-S-O ternary system were obtained by melting experiments up to 208 GPa
- O-rich, S-poor liquid iron alloy crystallizes solid Fe at the ICB
- The outer core can be a C-bearing, O-rich/S-poor liquid that is compatible with seismological observations

Supporting Information:
- Supporting Information S1

Correspondence to:
S. Yokoo,
shunpei@eps.s.u-tokyo.ac.jp

Citation:
Yokoo, S., Hirose, K., Sinmyo, R., & Tagawa, S. (2019). Melting experiments on liquidus phase relations in the Fe-S-O ternary system under core pressures. *Geophysical Research Letters*, *46*, 5137–5145. https://doi.org/10.1029/2019GL082277

Received 29 JAN 2019
Accepted 22 APR 2019
Accepted article online 29 APR 2019
Published online 16 MAY 2019

Abstract Melting experiments on the Fe-S-O ternary system were performed to 208 GPa in a laser-heated diamond-anvil cell. Compositions of liquids and coexisting solids in recovered samples were examined using a field-emission-type electron microprobe. The results demonstrate that the ternary eutectic point shifts toward the oxygen-rich, sulfur-poor side with increasing pressure, in accordance with changes in eutectic liquid compositions in the Fe-O and Fe-S binary systems. We also found that solid Fe crystallizing from liquid Fe-S-O does not include oxygen, while the partitioning of sulfur into solid Fe is enhanced with increasing pressure. These indicate that oxygen-rich, sulfur-poor liquid crystallizes Fe at the inner core boundary; however, it makes a large density difference between the liquid and solid core, which is inconsistent with observations. Alternatively, we found that a range of C-bearing, S-poor/O-rich liquids account for the density and velocity in the outer core and the density in the inner core.

Plain Language Summary Light elements in the Earth's core have not been identified yet. The core composition is constrained by the liquidus phase relations of iron alloyed with light elements at high pressure, because the outer core is crystallizing Fe that is depleted in light elements at the inner core boundary. The liquidus phase relations in ternary systems are sometimes different from those of binary systems but have been examined little under core pressures.
Sulfur and oxygen have been considered important light elements in the core. Here we performed melting experiments on Fe-S-O ternary alloys up to 208 GPa using a laser-heated diamond-anvil cell and determined the liquidus phase relations on the basis of textural/chemical characterizations of recovered samples. We also found that the partitioning of sulfur causes a small density contrast between coexisting solid and liquid, but oxygen makes a large difference. These results demonstrate that O-rich, S-poor liquid iron crystallizes Fe but causes a liquid/solid density contrast much larger than what is observed across the inner core boundary, suggesting that other light elements are required. Alternatively, we searched for possible liquid core compositions in Fe-S-O-Si and Fe-S-O-C and found a range of liquids in the latter system are compatible with seismological observations.

1. Introduction

The Earth's outer core is thought to be liquid iron alloyed with light elements, whose density is ~10% less than the density of pure iron (Birch, 1964). The density of the inner core is also smaller than that of pure iron by ~5% (Dewaele et al., 2006). In order to account for such density deficits for both the liquid outer core and the solid inner core, sulfur and oxygen have been proposed to be major light elements in the core (Hirose et al., 2013; Poirier, 1994), since sulfur is often found in iron meteorites and oxygen is least soluble to solid iron and can thus explain the density jump across the inner core boundary (ICB; Alfè et al., 2002). The concentrations of these two elements in the core have been argued repeatedly but remain controversial; shock compression measurements suggested S-rich, O-poor outer core liquid (Huang et al., 2011), while theoretical calculations favored S-poor, O-rich liquid (Badro et al., 2014; Umemoto et al., 2014). Recent density and sound velocity measurements of Fe-S alloys support the S-rich core (Kawaguchi et al., 2017; Morard et al., 2013).

The liquidus phase relation of iron alloys can constrain the outer core composition because the liquid core crystallizes the light-element-poor, solid inner core at the ICB. Earlier studies based on melting experiments to 254 GPa demonstrate that the eutectic liquid in the Fe-S binary system becomes more depleted in sulfur with increasing pressure and includes about 5 wt% S at the ICB pressure (Kamada et al., 2012; Mori et al., 2017). It indicates that sulfur is not a predominant light element in the core because liquid iron containing

5.8–14.0 wt% S, required to account for the density and velocity of the outer core (Badro et al., 2014; Kawaguchi et al., 2017; Morard et al., 2013; Umemoto et al., 2014), crystallizes solid enriched in sulfur more than the liquid. On the other hand, the oxygen content in the Fe-O binary eutectic liquid has been reported to be higher at higher pressures (Komabayashi, 2014; Morard et al., 2017; Seagle et al., 2008). Liquid iron alloy crystallizes Fe at 330 GPa, even when it includes more than 10 wt% O that is high enough to explain the outer core density deficit and velocity excess with respect to those of pure iron (Badro et al., 2014).

Previous experiments on the Fe-S-O ternary system were performed in a multianvil press to 21 GPa, focusing on the formation of two immiscible liquids (Tsuno et al., 2007; Urakawa et al., 1987). These studies demonstrated that a liquid-liquid immiscible region shrinks with increasing pressure, while thermodynamic modeling predicted liquid immiscibility still occurring in Fe-S-O at the outer core pressure range (Helffrich & Kaneshima, 2004). The melting temperature of 85%-13%S-2%O (in weight) was reported to 157 GPa by using a diamond-anvil cell (DAC) (Terasaki et al., 2011).

Here we performed melting experiments on Fe-S-O alloys up to 208 GPa and determined liquidus phase relations in the ternary system, in particular the liquidus fields of Fe, FeO, and Fe_3S from textural and chemical characterizations of recovered samples (Kamada et al., 2012; Mori et al., 2017; Ozawa et al., 2016). In addition, we also found that oxygen is not included in solid Fe crystallizing from liquid Fe-S-O, while solid/liquid partitioning of sulfur increases with increasing pressure. On the basis of these results, we argue the possible compositional range for the outer core in Fe-S-O and additionally in Fe-S-O-Si and Fe-S-O-C.

2. Experimental Methods

High-pressure and -temperature (*P-T*) conditions were generated using a laser-heated DAC (see Table S1 in the supporting information). Flat 300 μm, beveled 120 μm, or 90 μm culet diamond anvils were used. Starting materials were foils of homogeneous Fe-S-O with different S/O ratios, which were deposited on a glass slide by a sputtering method (Hirose et al., 2017); Fe-1.7wt%S-5.5wt%O and Fe-6.5wt%S-5.2wt%O (Figure S1 in the supporting information). The sample was loaded together with thermal insulation layers of Al_2O_3 into a hole at the center of a preindented rhenium gasket. After loading, a whole DAC was dried in a vacuum oven at 423 K, at least for 24 hr in order to eliminate moisture on the sample. Then, the sample was flushed with argon gas and subsequently compressed to a high pressure of interest in an argon atmosphere.

The sample was then heated from both sides with a couple of 100 W single-mode Yb fiber lasers. We employed beam-shaping optics, which converts a Gaussian beam to one with a flat energy distribution and thus diminishes the radial temperature gradient in a sample. The laser-heated spot was ~20 μm across. One-dimensional temperature distributions on the surface of the sample were obtained using a spectroradiometric method (e.g., Mori et al., 2017) (Figure 1c). Heating duration was limited to 3 s in order to avoid temperature fluctuation that could lead to a complex melting texture. Indeed, the quenched liquid pool was homogeneous in composition, indicating that both sulfur and oxygen diffused over the liquid pool in such a heating duration (Figures 1a–1c). Mori et al. (2017) conducted time-series experiments on an Fe-S sample and obtained similar results by changing heating duration from 1 to 120 s. It assures that 1 s is long enough to reach chemical equilibrium.

The temperature at the boundary between the liquid and the solid corresponds to crystallization temperature. Such a temperature was determined (Table S1 in the supporting information) by combining the melting texture found in a cross section of a sample with 1-D temperature profile across a heated spot considering that the liquid/solid boundary was isothermal (Figure 1c) (e.g., Hirose et al., 2017). In order to match the cross section and temperature profile, we obtained the widest molten area that should include the center of a heated spot. We measured pressure at 300 K after heating based on the Raman shift of diamond (Akahama & Kawamura, 2004). We corrected for thermal pressure contribution by following Andrault et al. (1998); for purely isochoric heating, the thermal pressure is written as $\Delta P = \alpha K_T \times T$, where α is thermal expansivity and K_T is isothermal bulk modulus. Ichikawa et al. (2014) estimated $\alpha K_T = 9$ MPa/K for liquid iron at 136 GPa and 4000 K, where 90% of the theoretical thermal pressure contributes to an increase in experimental pressure (Andrault et al., 1998). For runs #1 and #6 performed at relatively low pressures, the lower αK_T value of 4 MPa/K and 60% of the theoretical value were employed (Morard et al., 2011).

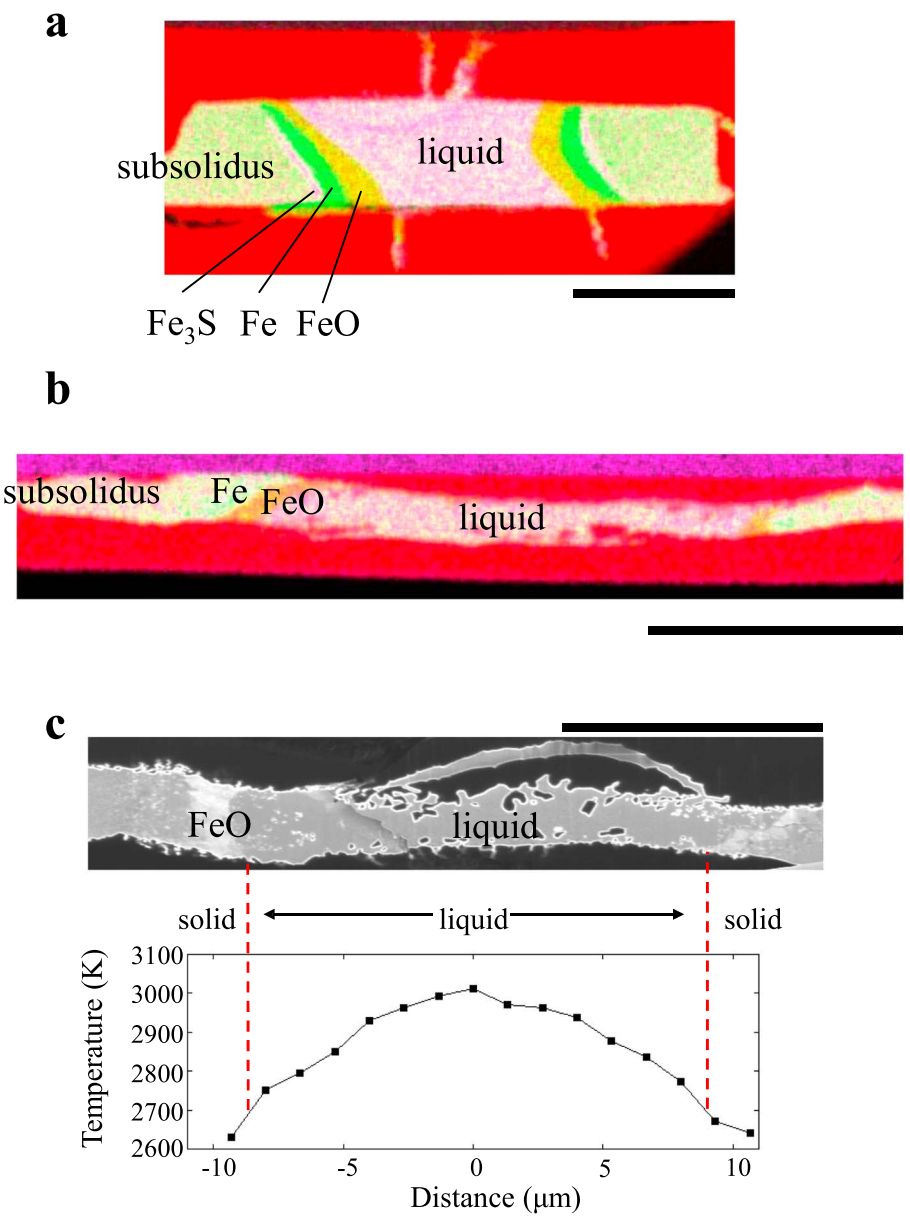

Figure 1. X-ray maps for iron (green), oxygen (red), and sulfur (purple) for sample cross sections parallel to the compression axis from (a) runs #6 at 53 GPa and (b) #3 at 202 GPa. (c) Scanning ion microscope image from run #5 performed at 130 GPa. Scale bars are 10 μm. Liquid pool is found at the center in contact with solid layers. Temperature at the liquid-solid boundary is given in (c), considering identical temperature for both sides.

The overall errors in temperature and pressure may be ±5% and ±10%, respectively, in the present experiments according to arguments on similar experiments performed by Mori et al. (2017).

Textural and chemical characterizations were carried out on all samples after they were recovered from a DAC. A cross section of the laser-heated portion was prepared parallel to a compression axis using a focused Ga ion beam (FIB) (FEI, Versa 3D DualBeam). The sample cross section was first examined by a field-emission (FE)-type scanning electron microscope (SEM) and an energy dispersive X-ray spectrometry (EDS) for X-ray elemental mapping. Subsequently, the chemical compositions of coexisting quenched liquid and solid phases were determined by FE-type electron probe micro analyzer, EPMA (JEOL, JXA-8530F) with an acceleration voltage of 12 kV and a beam current of 15 nA (Table S1 in the supporting information). While we found very minor amounts of Al in the EPMA analyses of liquids, it is most likely a signal derived

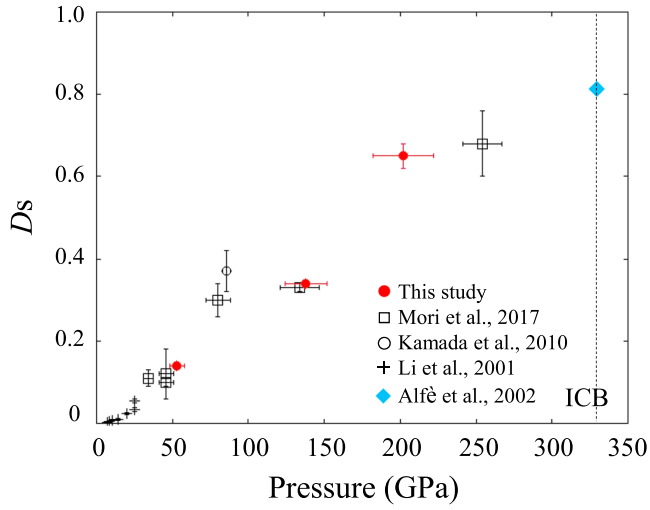

Figure 2. Solid/liquid partition coefficient for sulfur plotted as a function of pressure. Present results (red circles) are consistent with previous experimental (Kamada et al., 2010; Li et al., 2001; Mori et al., 2017) and theoretical studies (Alfè et al., 2002).

from neighboring/underlying Al_2O_3 insulation layers. We thus omitted aluminum and the corresponding amount of oxygen from raw data.

3. Results

3.1. Melting Textures

We have performed melting experiments at about 50, 135, and 200 GPa using two starting materials with different S/O ratios (Table S1 in the supporting information). In all the experiments, microprobe observations confirmed melting textures in their cross sections (Figures 1a–1c). There was a chemically homogeneous area at the center, the hottest part during laser heating. This area contained both sulfur and oxygen in addition to iron and is regarded as a quenched liquid. It is supported by the infiltration of Al_2O_3 grains from the surrounding pressure medium. The liquid immiscibility was not observed in any samples (Helffrich & Kaneshima, 2004; Urakawa et al., 1987). Solid layers are found in the outer region where temperature was lower, in contact with a quenched liquid part (Figure 1c). Each solid layer included a single phase; we always found an FeO layer in addition to the layer of Fe or Fe_3S (or both) (Table S1 in the supporting information). The solid Fe contained some sulfur but no oxygen (see below). These crystals coexisting with liquid are interpreted to be liquidus phases; see Ito et al. (2004) for the interpretation of melting texture obtained in multianvil experiments and Mori et al. (2017) for DAC samples. While two kinds of the liquidus phases were observed in run #1–4, three crystals (Fe, FeO, and Fe_3S) coexisted with the liquid in run #6 (Figure 1a). The liquids in the former should represent cotectic liquids, whereas the latter one is a ternary eutectic liquid. The liquid only coexisted with FeO in run #5. Its composition should therefore be within the liquidus field of FeO but is most likely close to the cotectic line as observed in other runs. Outside of these liquidus phase layers, we found a subsolidus part whose composition was identical to that of the starting material.

3.2. Solid/Liquid Partitioning of Sulfur and Oxygen

Partition coefficients of sulfur between coexisting solid Fe and liquid Fe-S-O, D_S (defined as solid/liquid), were obtained in the present experiments. The D_S values are also found in earlier high-pressure experimental studies on the Fe-FeS binary system (Kamada et al., 2010, 2012; Li et al., 2001; Mori et al., 2017; Stewart et al., 2007). All data are consistent with each other when plotted as a function of pressure (Figure 2), suggesting that oxygen does not affect the solid/liquid partitioning of sulfur. Temperature effect on D_S is likely to be small as illustrated previously in the Fe–Fe_3S binary phase diagram (e.g., Kamada et al., 2010).

The partitioning of sulfur into solid Fe is strongly enhanced with increasing pressure from D_S = ~0.0 at 20 GPa to ~0.7 at 250 GPa (Figure 2). The linear extrapolation suggests D_S = ~0.8 at 330 GPa, in good agreement with the previous prediction by Alfè et al. (2002).

In contrast, the present EPMA analyses did not show any oxygen in solid Fe. The absence of oxygen in solid Fe is consistent with the previous observation by Ozawa et al. (2010) to 197 GPa and 3600 K. An O-rich core composition thus makes a large density difference between the liquid and solid core.

3.3. Liquidus Phase Relations in Fe-S-O

Except for run #5, liquids obtained in this study coexisted with two or three solid phases (examples shown in Figures 1a and 1b) (Table S1 in the supporting information) and therefore represent those of the Fe + FeO or FeO + Fe_3S cotectic, or of the Fe-FeO-Fe_3S eutectic in the ternary system. The Fe-FeO and Fe-Fe_3S binary eutectic liquid compositions have been experimentally examined at high pressures to 105 GPa (Morard et al., 2017) and 254 GPa (Mori et al., 2017), respectively.

Figures 3a–3c illustrate the liquidus phase (the first crystallizing solid phase) relations in the Fe-S-O system at about 50, 135, and 200 GPa, constrained by these liquid compositions and coexisting phases. The position of the Fe + FeO cotectic line (showing liquid compositions coexisting with both Fe and FeO) moves toward the oxygen-rich side with increasing pressure from 50 to 135 GPa (Figure 3d), consistent with the earlier

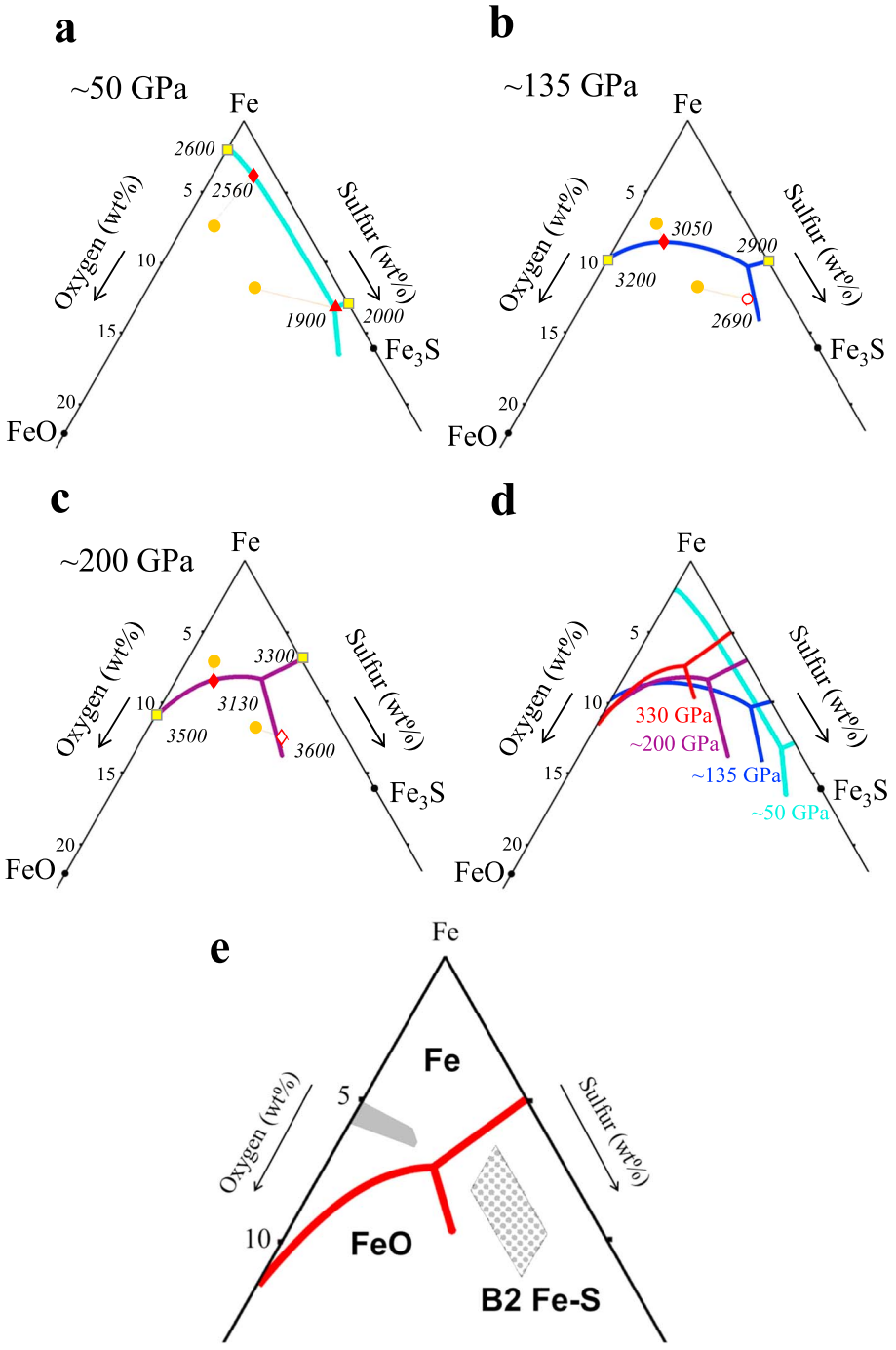

Figure 3. (a–c) Liquidus phase relations in the Fe-S-O system at (a) ~50, (b) ~135, and (c) ~200 GPa. Liquids coexisted with Fe+FeO+Fe_3S (triangle), Fe+FeO (filled diamonds), Fe+Fe_3S (open diamond), or FeO only (open circle). The compositions of starting materials are shown by orange filled circles. The Fe-Fe_3S (Mori et al., 2017) and Fe-FeO (Morard et al., 2017) binary eutectic liquid compositions are also plotted (yellow squares). Three curves illustrate cotectic lines at each pressure derived from the present results. Numbers indicate temperatures. (d) The change in liquidus phase relations with increasing pressure. (e)The ranges of Fe-S-O liquid core composition proposed by Badro et al. (2014) (shaded area) based on the density and bulk sound velocity of the outer core and by Alfè et al. (2002) (dotted area) from the densities of the outer and inner cores. The liquidus phase relations (red lines) are for 330 GPa.

observations by Morard et al. (2017) that show the oxygen concentration in the Fe-FeO binary eutectic liquid increases substantially above 80 GPa. On the other hand, the Fe + Fe_3S cotectic shifts toward the sulfur-poor side, reflecting the depletion in sulfur content in the Fe-Fe_3S binary eutectic liquid with increasing pressure (Kamada et al., 2012; Mori et al., 2017).

The position of the ternary eutectic point at ~50 GPa was directly obtained from the liquid composition that coexisted with Fe + FeO + Fe_3S. At ~135 and ~200 GPa, it was estimated from cotectic lines and the binary eutectic points considering the liquidus temperature found in each run. The ternary eutectic point is located on the sulfur-rich side at 50 GPa and shifts toward the oxygen-rich side with increasing pressure (Figure 3d). It is controlled by the difference in eutectic melting temperature between the Fe-FeO and the Fe-Fe_3S binary systems; the latter is much lower than the former around 50 GPa but becomes closer with increasing pressure (Morard et al., 2017; Mori et al., 2017). We also found that the ternary eutectic point is located close to the tie-line directly connecting the Fe-FeO and the Fe-Fe_3S binary eutectic points. A similar observation was made in the Fe-Si-S ternary system by Tateno et al. (2018).

Crystallization temperatures determined in our experiments are consistent with the binary eutectic temperatures in Fe-FeO and Fe-Fe_3S (Morard et al., 2017; Mori et al., 2017) (Figures 3a–3c). At ~50 GPa, the ternary minimum is close in both composition and temperature to the Fe-Fe_3S binary eutectic point. At higher pressures, the ternary eutectic temperatures are not tightly constrained, but the present results suggest that the Fe-S-O ternary eutectic melting curve has a smaller temperature/pressure slope than the Fe-Fe_3S binary eutectic (Kamada et al., 2012; Mori et al., 2017; Terasaki et al., 2011).

4. Fe-S-O Core?

4.1. Constraint From Liquidus Phase Relations

The density jump across the ICB has been estimated to be 0.55–0.82 g/cm^3 (Dziewonski & Anderson, 1983; Masters & Gubbins, 2003; Shearer & Masters, 1990). It is more than the density change by 0.15–0.20 g/cm^3 upon the melting of iron at 330 GPa (Ichikawa et al., 2014), suggesting that the solid inner core contains lower amounts of light elements than the liquid outer core. In order for the inner core to be depleted in the light elements, the liquid core composition should be within the liquidus field of Fe (the compositional range from which Fe first crystallizes), rather than that of FeO or B2-type Fe-S (Fe_3S is not stable above 250 GPa) (Mori et al., 2017; Ozawa et al., 2013), at 330 GPa.

Present experiments demonstrate that both the Fe + FeO and Fe + Fe_3S cotectic lines that define the liquidus field of Fe are located close to the direct tie-line between the binary eutectic points in the Fe-Fe_3S and Fe-FeO systems (Figures 3a–3c). This is similar to the case observed in Fe-Si-S (Tateno et al., 2018). Based on this observation and the binary eutectic liquid compositions inferred from previous studies (Komabayashi, 2014; Morard et al., 2017; Mori et al., 2017), we estimate the liquidus field of Fe in the Fe-S-O ternary at 330 GPa, which extends to relatively S-poor and O-rich compositions (Figure 3d). Although our experiments were performed below the decomposition pressure of Fe_3S (Ozawa et al., 2013), it does not cause a discontinuous jump in the eutectic liquid composition and should not change our estimate of the eutectic composition at 330 GPa remarkably (Mori et al., 2017).

Badro et al. (2014) argued that the outer core is sulfur-poor (0–2 wt% S) and oxygen-rich (4–5.5 wt% O) in order to account for seismological observations of its density and bulk sound velocity when S and O are the core light elements. Such liquid compositions are fully within the liquidus field of Fe at the ICB pressure (Figure 3e) and can thus crystallize solids depleted in S and O.

Indeed, the S-poor core composition is supported by cosmochemical and geochemical arguments. The high volatility of sulfur may limit its bulk Earth abundance and accordingly its concentration in the core to 1.2 to 1.9 wt% (Allègre et al., 2001; Dreibus & Palme, 1996; McDonough, 2014). Recent metal-silicate partitioning experiments also suggested that the sulfur content in the core is below ~2 wt% (Suer et al., 2017).

4.2. Constraint From Density Jump Across ICB

Our new data combined with previous ones (Kamada et al., 2010; Li et al., 2001; Mori et al., 2017) show that the solid/liquid partitioning of sulfur, $D_S = 0.8$ when extrapolating the experimental data to 330 GPa (Figure 2), is in good agreement with the earlier theoretical prediction by Alfè et al. (2002). Sulfur,

therefore, contributes little to the density jump across the ICB. In contrast, oxygen is not partitioned into solid Fe. An O-rich core composition thus makes a large difference in density between the liquid and solid core.

The ab initio calculations by Alfè et al. (2002) demonstrated that the oxygen content in the outer core is limited to 2.5 wt%; otherwise, the density jump across the ICB will be too large. The S-poor (0–2 wt% S), O-rich (4–5.5 wt% O) liquid core, proposed by Badro et al. (2014) on the basis of the density and bulk sound velocity of the outer core, may therefore be unlikely. Alfè and others estimated S-rich (6.4 wt%), O-poor (2.5 wt%) liquid core composition (Figure 3e) to explain the densities of both the outer and inner core. However, such S-rich, O-poor liquid core is not verified by the present experiments; it crystallizes S-rich Fe-S alloy (B2-type phase) (Mori et al., 2017; Ozawa et al., 2013) and thus cannot form the inner core that is denser than the outer core. The outer core should, therefore, include other light elements in addition to sulfur and oxygen.

4.3. Presence of Carbon

We searched for possible liquid core compositions in Fe-S-O-Si and Fe-S-O-C, which satisfy both the constraints from the density and sound velocity in the outer core and from the ICB density jump (i.e., the inner core density). The liquidus field of Fe in these quaternary systems is estimated by considering the Fe-FeSi (Ozawa et al., 2016) and Fe-C binary eutectic compositions (Mashino et al., 2019). The present experiments on Fe-S-O as well as those by Tateno et al. (2018) on Fe-Si-S show that the liquidus field of Fe is approximated by a tie-line connecting the relevant binary eutectic points. We assume it is true for the Fe-S-O-Si and Fe-S-O-C systems. The S, Si, and C contents in solid Fe crystallizing at the ICB are obtained from $D_S = 0.8$ (see above), $D_{Si} = 1.0$ (Alfè et al., 2002), and $D_C = 0.33$ (Mashino et al., 2019). The compositional range in solid Fe-S-Si and Fe-S-C that explains the observed inner core density has been demonstrated by the recent calculations by Li et al. (2018).

First, we found that the Fe-S-O-Si liquid core is not possible, in major part because the eutectic liquid in the Fe-FeSi system includes only <1.5 wt% Si under the core pressure range (Ozawa et al., 2016). On the other hand, C-bearing, S-poor/O-rich liquids meet the above criteria. With 1 wt% C, liquid Fe-2.2wt%S-2.7wt%O-1.0wt%C ($Fe_{84.0}S_{3.4}O_{8.4}C_{4.2}$) crystallizes solid Fe-1.8wt%S-0.3wt%C whose density is 13.28 ± 0.06 g/cm^3 at 360 GPa and 6000 K according to Li et al. (2018). It is approximately consistent with the corresponding inner core density of 13.05 g/cm^3 when considering the uncertainty of 0.1–0.2 g/cm^3 in the PREM (Souriau & Calvet, 2015). With 2 wt% C, liquid Fe-0.7wt%S-2.5wt%O-2.0wt%C ($Fe_{83.2}S_{1.1}O_{8.2}C_{7.5}$) forms solid Fe-0.6wt%S-0.7wt%C with a density of 13.30 ± 0.07 g/cm^3, which also matches the observation within their uncertainties. In addition, the calculations by Umemoto and Hirose (2015) suggested the presence of hydrogen is compatible with the density and velocity of the outer core. Phase relations of hydrogen-bearing Fe alloy systems and the property of solid Fe-H remain to be explored.

5. Conclusions

Present melting experiments examined the change in liquidus phase relations in the Fe-S-O ternary system with increasing pressure to 208 GPa. We found that (1) the ternary eutectic point is located close to the tie-line directly connecting the Fe-FeO and Fe-Fe_3S binary eutectic points at each pressure and (2) the liquidus field of Fe becomes more enriched in oxygen and depleted in sulfur with increasing pressure. The results also show that (3) the solid/liquid partition coefficient of sulfur increases at higher pressures and is D_S (solid/liquid) = ~0.8 at 330 GPa, in good agreement with previous theoretical predictions by Alfè et al. (2002). On the other hand, our EPMA analyses did not show any oxygen in solid Fe that crystallized from liquid Fe-S-O.

The liquidus phase relations constrain the possible range of liquid core composition in Fe-S-O to be S-poor and O-rich, since the inner core consists of solid Fe rather than the S-rich B2 phase (Mori et al., 2017; Ozawa et al., 2013) or FeO. The liquidus field of Fe at 330 GPa fully covers the range of Fe-S-O liquid core compositions that are S-poor (0–2 wt% S) and O-rich (4–5.5 wt% O), which explain the density and velocity of the outer core (Badro et al., 2014). Nevertheless, oxygen-rich liquid core causes too large of a density contrast between the outer and the inner core when it includes more than ~3 wt% O, suggesting the presence of the other light element in the core in addition to S and O. We found that a range of C-bearing, S-poor/O-rich liquids meet all of these constraints, considering the recent calculations on solid Fe alloys by Li et al. (2018).

Acknowledgments

Data for Figures 2 and 3 are given in Table S1 in the supporting information. We thank K. Yonemitsu for help in sample analyses with focused Ga ion beam, energy dispersive X-ray spectrometry, and EPMA. Comments from the reviewers were helpful to improve the manuscript.

References

Akahama, Y., & Kawamura, H. (2004). High-pressure Raman spectroscopy of diamond anvils to 250 GPa: Method for pressure determination in the multimegabar pressure range. *Journal of Applied Physics*, *96*(7), 3748–3751. https://doi.org/10.1063/1.1778482

Alfè, D., Gillan, M. J., & Price, G. D. (2002). Composition and temperature of the Earth's core constrained by combining ab initio calculations and seismic data. *Earth and Planetary Science Letters*, *195*(1–2), 91–98. https://doi.org/10.1016/S0012-821X(01)00568-4

Allègre, C., Manhès, G., & Lewin, É. (2001). Chemical composition of the Earth and the volatility control on planetary genetics. *Earth and Planetary Science Letters*, *185*(1-2), 49–69. https://doi.org/10.1016/S0012-821X(00)00359-9

Andrault, D., Fiquet, G., Itie, J. P., Richet, P., Gillet, P., Hausermann, D., & Hanfland, M. (1998). Thermal pressure in the laser-heated diamond-anvil cell: An X-ray diffraction study. *European Journal of Mineralogy*, *10*(5), 931–940. https://doi.org/10.1127/ejm/10/5/0931

Badro, J., Cote, A. S., & Brodholt, J. P. (2014). A seismologically consistent compositional model of Earth's core. *Proceedings of the National Academy of Sciences of the United States of America*, *111*(21), 7542–7545. https://doi.org/10.1073/pnas.1316708111

Birch, F. (1964). Density and composition of mantle and core. *Journal of Geophysical Research*, *69*(20), 4377–4388. https://doi.org/10.1029/JZ069i020p04377

Dewaele, A., Loubeyre, P., Occelli, F., Mezouar, M., Dorogokupets, P. I., & Torrent, M. (2006). Quasihydrostatic equation of state of Iron above 2 Mbar. *Physical Review Letters*, *97*(21), 29–32. https://doi.org/10.1103/PhysRevLett.97.215504

Dreibus, G., & Palme, H. (1996). Cosmochemical constraints on the sulfur content in the Earth's core. *Geochimica et Cosmochimica Acta*, *60*(7), 1125–1130. https://doi.org/10.1016/0016-7037(96)00028-2

Dziewonski, A. M., & Anderson, D. L. (1983). Travel times and station corrections for *P* waves at teleseismic distances. *Journal of Geophysical Research*, *88*(B4), 3295–3314. https://doi.org/10.1029/JB088iB04p03295

Helffrich, G., & Kaneshima, S. (2004). Seismological constraints on core composition from Fe-O-S liquid immiscibility. *Science*, *306*(5705), 2239–2242. https://doi.org/10.1126/science.1101109

Hirose, K., Labrosse, S., & Hernlund, J. (2013). Composition and state of the core. *Annual Review of Earth and Planetary Sciences*, *41*(1), 657–691. https://doi.org/10.1146/annurev-earth-050212-124007

Hirose, K., Morard, G., Sinmyo, R., Umemoto, K., Hernlund, J., Helffrich, G., & Labrosse, S. (2017). Crystallization of silicon dioxide and compositional evolution of the Earth's core. *Nature*, *543*(7643), 99–102. https://doi.org/10.1038/nature21367

Huang, H., Fei, Y., Cai, L., Jing, F., Hu, X., Xie, H., et al. (2011). Evidence for an oxygen-depleted liquid outer core of the Earth. *Nature*, *479*(7374), 513–516. https://doi.org/10.1038/nature10621

Ichikawa, H., Tsuchiya, T., & Tange, Y. (2014). The P-V-T equation of state and thermodynamic properties of liquid iron. *Journal of Geophysical Research: Solid Earth*, *119*, 240–252. https://doi.org/10.1002/2013JB010732

Ito, E., Kubo, A., Katsura, T., & Walter, M. J. (2004). Melting experiments of mantle materials under lower mantle conditions with implications for magma ocean differentiation. *Physics of the Earth and Planetary Interiors*, *143-144*(1–2), 397–406. https://doi.org/10.1016/j.pepi.2003.09.016

Kamada, S., Ohtani, E., Terasaki, H., Sakai, T., Miyahara, M., Ohishi, Y., & Hirao, N. (2012). Melting relationships in the Fe-Fe_3S system up to the outer core conditions. *Earth and Planetary Science Letters*, *359-360*, 26–33. https://doi.org/10.1016/j.epsl.2012.09.038

Kamada, S., Terasaki, H., Ohtani, E., Sakai, T., Kikegawa, T., Ohishi, Y., et al. (2010). Phase relationships of the Fe-FeS system in conditions up to the Earth's outer core. *Earth and Planetary Science Letters*, *294*(1–2), 94–100. https://doi.org/10.1016/j.epsl.2010.03.011

Kawaguchi, S. I., Nakajima, Y., Hirose, K., Komabayashi, T., Ozawa, H., Tateno, S., et al. (2017). Sound velocity of liquid Fe-Ni-S at high pressure. *Journal of Geophysical Research: Solid Earth*, *122*, 3624–3634. https://doi.org/10.1002/2016JB013609

Komabayashi, T. (2014). Thermodynamics of melting relations in the system Fe-FeO at high pressure: Implications for oxygen in the Earth's core. *Journal of Geophysical Research: Solid Earth*, *119*, 4164–4177. https://doi.org/10.1002/2014JB010980

Li, J., Fei, Y., Mao, H. K., Hirose, K., & Shieh, S. R. (2001). Sulfur in the Earth's inner core. *Earth and Planetary Science Letters*, *193*(3-4), 509–514. https://doi.org/10.1016/S0012-821X(01)00521-0

Li, Y., Vočadlo, L., & Brodholt, J. P. (2018). The elastic properties of hcp-Fe alloys under the conditions of the Earth's inner core. *Earth and Planetary Science Letters*, *493*, 118–127. https://doi.org/10.1016/j.epsl.2018.04.013

Mashino, I., Miozzi, F., Hirose, K., Morard, G., & Sinmyo, R. (2019). Melting experiments on the Fe-C binary system up to 255 GPa: Constraints on the carbon content in the Earth's core. *Earth and Planetary Science Letters*, *515*, 135–144. https://doi.org/10.1016/j.epsl.2019.03.020

Masters, G., & Gubbins, D. (2003). On the resolution of density within the Earth. *Physics of the Earth and Planetary Interiors*, *140*(1–3), 159–167. https://doi.org/10.1016/j.pepi.2003.07.008

McDonough, W. F. (2014). Compositional model for the Earth's core. In R. W. Carlson, H. D. Holland, & K. K. Turekian (Eds.), *Treatise on Geochemistry*, (3rd ed., Vol. 3, pp. 559–577). Amsterdam: Elsevier. https://doi.org/10.1016/B978-0-08-095975-7.00215-1

Morard, G., Andrault, D., Antonangeli, D., Nakajima, Y., Auzende, A. L., Boulard, E., et al. (2017). Fe-FeO and Fe-Fe_3C melting relations at Earth's core–mantle boundary conditions: Implications for a volatile-rich or oxygen-rich core. *Earth and Planetary Science Letters*, *473*, 94–103. https://doi.org/10.1016/j.epsl.2017.05.024

Morard, G., Andrault, D., Guignot, N., Siebert, J., Garbarino, G., & Antonangeli, D. (2011). Melting of Fe–Ni–Si and Fe–Ni–S alloys at megabar pressures: Implications for the core–mantle boundary temperature. *Physics and Chemistry of Minerals*, *373*(10), 169–178. https://doi.org/10.1016/j.epsl.2013.04.040

Morard, G., Siebert, J., Andrault, D., Guignot, N., Garbarino, G., Guyot, F., & Antonangeli, D. (2013). The Earth's core composition from high pressure density measurements of liquid iron alloys. *Earth and Planetary Science Letters*, *373*, 169–178. https://doi.org/10.1016/j.epsl.2013.04.040

Mori, Y., Ozawa, H., Hirose, K., Sinmyo, R., Tateno, S., Morard, G., & Ohishi, Y. (2017). Melting experiments on Fe-Fe_3S system to 254 GPa. *Earth and Planetary Science Letters*, *464*, 135–141. https://doi.org/10.1016/j.epsl.2017.02.021

Ozawa, H., Hirose, K., Suzuki, T., Ohishi, Y., & Hirao, N. (2013). Decomposition of Fe_3S above 250 GPa. *Geophysical Research Letters*, *40*, 4845–4849. https://doi.org/10.1002/grl.50946

Ozawa, H., Hirose, K., Tateno, S., Sata, N., & Ohishi, Y. (2010). Phase transition boundary between B1 and B8 structures of FeO up to 210 GPa. *Physics of the Earth and Planetary Interiors*, *179*(3-4), 157–163. https://doi.org/10.1016/j.pepi.2009.11.005

Ozawa, H., Hirose, K., Yonemitsu, K., & Ohishi, Y. (2016). High-pressure melting experiments on Fe–Si alloys and implications for silicon as a light element in the core. *Earth and Planetary Science Letters*, *456*, 47–54. https://doi.org/10.1016/j.epsl.2016.08.042

Poirier, J. P. (1994). Light elements in the Earth's outer core: A critical review. *Physics of the Earth and Planetary Interiors*, *85*(3-4), 319–337. https://doi.org/10.1016/0031-9201(94)90120-1

Seagle, C. T., Heinz, D. L., Campbell, A. J., Prakapenka, V. B., & Wanless, S. T. (2008). Melting and thermal expansion in the Fe-FeO system at high pressure. *Earth and Planetary Science Letters*, *265*(3-4), 655–665. https://doi.org/10.1016/j.epsl.2007.11.004

Shearer, P., & Masters, G. (1990). The density and shear velocity contrast at the inner core boundary. *Geophysical Journal International*, *102*(2), 491–498. https://doi.org/10.1111/j.1365-246X.1990.tb04481.x

Souriau, A., & Calvet, M. (2015). Deep Earth structure: The Earth's cores. In A. M. Dziewonski, B. A. Romanowicz, & G. Schubert (Eds.), *Treatise on Geophysics*, (2nd ed., Vol. 1, pp. 725–757). Amsterdam: Elsevier. https://doi.org/10.1016/B978-0-444-53802-4.00020-8

Stewart, A. J., Schmidt, M. W., van Westrenen, W., & Liebske, C. (2007). Mars: A new core-crystallization regime. *Science*, *316*(5829), 1323–1325. https://doi.org/10.1126/science.1140549

Suer, T., Siebert, J., Remusat, L., Menguy, N., & Fiquet, G. (2017). A sulfur-poor terrestrial core inferred from metal-silicate partitioning experiments. *Earth and Planetary Science Letters*, *469*, 84–97. https://doi.org/10.1016/j.epsl.2017.04.016

Tateno, S., Hirose, K., Sinmyo, R., Morard, G., Hirao, N., & Ohishi, Y. (2018). Melting experiments on Fe–Si–S alloys to core pressures: Silicon in the core? *American Mineralogist*, *103*(5), 742–748. https://doi.org/10.2138/am-2018-6299

Terasaki, H., Kamada, S., Sakai, T., Ohtani, E., Hirao, N., & Ohishi, Y. (2011). Liquidus and solidus temperatures of a Fe-O-S alloy up to the pressures of the outer core: Implication for the thermal structure of the Earth's core. *Earth and Planetary Science Letters*, *304*(3-4), 559–564. https://doi.org/10.1016/j.epsl.2011.02.041

Tsuno, K., Ohtani, E., & Terasaki, H. (2007). Immiscible two-liquid regions in the Fe-O-S system at high pressure: Implications for planetary cores. *Physics of the Earth and Planetary Interiors*, *160*(1), 75–85. https://doi.org/10.1016/j.pepi.2006.09.004

Umemoto, K., & Hirose, K. (2015). Liquid iron-hydrogen alloys at outer core conditions by first-principles calculations. *Geophysical Research Letters*, *42*, 7513–7520. https://doi.org/10.1002/2015GL065899

Umemoto, K., Hirose, K., Imada, S., Nakajima, Y., Komabayashi, T., Tsutsui, S., & Baron, A. Q. (2014). Liquid iron-sulfur alloys at outer core conditions by first-principles calculations. *Geophysical Research Letters*, *41*, 6712–6717. https://doi.org/10.1002/2014GL061233

Urakawa, S., Kato, M., & Kumazawa, M. (1987). Experimental study on the phase relations in the system Fe-Ni-O-S up to 15 GPa. In M. H. Manghnami, & Y. Shono (Eds.), *High-Pressure Research in Mineral Physics: A Volume in Honor of Syun-iti Akimoto*, (pp. 95–111). Tokyo: Terrapub/Washington, DC: American Geophysical Union. https://doi.org/10.1029/GM039p0095